JSST
Journal of Space Science and Technology

P-ISSN: 2008-4560
E-ISSN: 2423-4516

Journal of Space Science and Technology

Vol. ??, No. ?, pp.1-9, 2026
https://doi.org/10.22034/jsst.2025.1568
Journal Homepage: https://jsstpub.com

Original Research Paper

Numerical Investigation of Cavitation Reduction Around a 2D Hydrofoil by Water Injection Using the VOF Method and LES Turbulence Model

Yasin Ebrahimi[1], Soheil Motezakkeri [2], Amirmehran Mahdavi[3*], Ali Alavi[4], and Ehsan Roohi [5]

1,2. Department of Aerospace Engineering, Hakim Sabzevari University, Sabzevar, Iran
3. Department of Mechanical Engineering, Hakim Sabzevari University, Sabzevar, Iran
4. Department of Mechanical Engineering, Ferdowsi University of Mashhad, Mashhad, Iran
5. Department of Aerospace Engineering, Embry-Riddle Aeronautical University, Florida, United States

ARTICLE INFO

Article History:

Received 10 August 2025
Revised 07 November 2025
Accepted 07 November 2025
Available Online 09 November 2025

Keywords:

Injection
Hydrofoil Clark-Y
Cloud cavitation
VOF model
LES turbulence

ABSTRACT

This article focuses on the mitigation of cavitation in fluid flow under specified velocity conditions. A Clark-Y hydrofoil with a 70 mm chord length is designed to emulate a fish-gill-inspired configuration aimed at suppressing unsteady cavitation phenomena. Jet injection with a velocity of 0.5 $U\infty$ is implemented at 15% and 60% of the chord length on the hydrofoil surface under an 8-degree angle of attack. The jet is aligned parallel to the mainstream flow. The flow is modeled using the multiphase implicit volume of fluid (VOF) method coupled with the large eddy simulation (LES) turbulence model to accurately capture the transient behavior of cavitating flow. Simulations are performed at a cavitation number of $\sigma = 0.8$ and a Reynolds number of 7×10^5. The numerical findings demonstrate that jet injection effectively stabilizes the cavity shedding process and reduces the amplitude of pressure fluctuations on the hydrofoil surface. The injection at 15% chord length not only decreases cavity length but also delays the onset of cloud cavitation, resulting in a smoother pressure recovery and enhanced hydrodynamic performance. In contrast, injection at 60% chord length provides localized suppression of trailing-edge cavitation without significantly affecting leading-edge dynamics. Overall, the study highlights the capability of controlled jet injection as an efficient passive method for mitigating unsteady cavitation and improving flow stability around hydrofoils.

* Corresponding Author's E-mail: am.me.mahdavi@gmail.com

How to Cite this Article:
Y. Ebrahimi, S. Motezakkeri, A. Mahdavi, A. Alavi, and Ehsan Roohi 5, "Numerical investigation of cavitation reduction around a 2D hydrofoil by water injection using the VOF method and LES turbulence model," *Journal of Space Science and Technology*, Vol. ??, No. ?, pp. 1-9, 2026, https://doi.org/10.22034/jsst.2025.1568.

1. INTRODUCTION

Cavitation, a phenomenon where local pressure drops below the vapor saturation pressure in a liquid, leads to the formation and collapse of vapor bubbles, causing potential damage to mechanical components such as hydrofoils through shock waves generated during bubble collapse. This study investigates the suppression of unsteady cavitation around a two-dimensional Clark-Y hydrofoil, inspired by the gill slit structures of aquatic organisms like sharks, which are known for their streamlined efficiency in high-speed aquatic environments. By incorporating jet injection at strategic positions (15% and 60% of the chord length) on the hydrofoil surface, this research aims to mitigate cavitation under specific flow conditions, characterized by a cavitation number of σ=0.8 and a Reynolds number of 7×10^5. The jet injection, set at 0.5 times the freestream velocity and aligned with the mainstream flow, enhances the boundary layer thickness, reducing velocity gradients and shear stress, thereby aiding cavitation control. The numerical simulations employ the implicit Volume of Fluid (VOF) method coupled with the Large Eddy Simulation (LES) turbulence model, implemented in ANSYS Fluent, to accurately capture the transient multiphase flow dynamics. The LES approach, which resolves large-scale eddies while modeling smaller dissipative scales, has proven effective in predicting cavitation details, surpassing traditional two-equation turbulence models like k-ε and k-ω [1-5]. The LES approach directly resolves large, energy-containing eddies that strongly interact with vapor structures, making it particularly suitable for capturing unsteady phenomena such as cavity shedding, re-entrant jet formation, and pressure shock waves generated during cavity collapse [6, 7]. Moreover, LES is frequently combined with cavitation mass-transfer models such as Zwart–Gerber–Belamri (ZGB) or Schnerr–Sauer to achieve accurate representation of vapor–liquid phase interactions [8, 9]. For example, long et al. [10] applied LES coupled with a homogeneous cavitation model to investigate turbulent cavitating flow around a sphere, successfully reproducing complex vortex dynamics and the evolution of cavity shedding. Various cavitation models, such as those based on the Rayleigh equation,[11-12] and semi-analytical mass transfer formulations [13], have been proposed to improve simulation accuracy. Recently, Li et al. [14] investigated the suppression of unsteady cavitation around a Clark-Y hydrofoil using periodic, time-varying jets inspired by fish gill respiration. Their work focused on analyzing different jet modulation patterns and their influence on re-entrant jet dynamics. In contrast, the present study explores steady jet injection at various chordwise positions. This approach is intentionally adopted to first isolate and fundamentally understand the influence of the jet's spatial location on cavitation dynamics, independent of the complexities of time-varying control. By establishing this necessary baseline, our work provides complementary insights to studies like Li et al. [14], focusing on *where* injection is most effective before exploring *how* (e.g., periodically) it is applied. This study, therefore, analyzes the impact of jet positioning on flow stability and pressure distribution to optimize the suppression mechanism.

The principle of jet-flow interaction is a broad control strategy applied across various fluid dynamics domains. Studies in other fields, for instance, have investigated the benefits of injection for flow stabilization and control [15]. A shared theme across these applications is the significant computational challenge associated with accurately modeling the complex, multi-scale physics of the interaction zone, which often involves high gradients and non-equilibrium turbulence [16-17] Our work addresses these concepts in the specific context of mitigating unsteady cavitation.

2. Governing equations

The cavitation boundary, marking the transition between vapor and liquid, defines the free surface. By applying linear conservation principles to a fluid control volume, using a general velocity from fundamental displacement theory, we arrive at governing equations that include continuity, Navier-Stokes momentum, and liquid volume fraction [12]. Cavitation, the vaporization that happens when pressure falls below vapor pressure, makes the fluid compressible. However, because vapor bubbles often occupy a small volume, the overall liquid flow in practical scenarios tends to remain relatively incompressible. This allows us to assume incompressible flow, even with cavitation, to simplify the analysis of global flow features. This simplification yields accurate results for pressure distribution, object forces, and flow patterns. The

continuity and momentum equations are then clarified.

$$\vec{\nabla}.\vec{u} = \dot{m}(\frac{1}{\rho_\iota} - \frac{1}{\rho_\vartheta}) \quad (1)$$

$$\frac{\partial}{\partial t}(\rho\vec{u}) + \vec{\nabla}.(\rho\vec{u}\vec{u}) = -\vec{\nabla}p + 2\vec{\nabla}.[\mu\vec{D}] + \rho\vec{g} + \sigma\kappa\vec{\nabla}\gamma_1 \quad (2)$$

In the presented equations, the variable $\vec{u}$ (m/s) velocity, P (Pa) denotes pressure, and the variable $\vec{g}$ (m/s^2) stands for gravitational acceleration. Furthermore, the magnitude of the shear stress tensor is articulated by the following formula [18]:

$$\vec{\vec{D}} = \frac{1}{2}\left[\vec{\nabla}\vec{u} + (\vec{\nabla}\vec{u})^T\right] \quad (3)$$

The equations in current study are based on the assumption of incompressible phases sharing a common initial velocity. Here, $\vec{u}$ (m/s) represents the magnitude of the time-averaged mixture velocity, P(Pa) is the time averaged pressure, and $\dot{m}$ (kg/s) denotes the mass transfer rate during cavitation phase change. The coefficient μ_t (Pas) represents the turbulence viscosity, while γ_ι (no unit) and γ_ϑ (no unit) are the volume fractions of liquid and vapor, respectively. These volume fractions are precisely defined by the following expressions:

$$\gamma_\iota = \frac{\dot{m}_\iota}{\dot{m}_{Total}} \quad (4)$$

$$\gamma_\vartheta = \frac{\dot{m}_\vartheta}{\dot{m}_{Total}} \quad (5)$$

In equations (4) and (5), the represents $\dot{m}_{Total}$ (kg/s) denotes the total mass flow rate and is defined as follows:

$$\dot{m}_{Total} = \dot{m}_\iota + \dot{m}_\vartheta \quad (6)$$

Consequently, μ (Pas) and ρ (kg/m^3) respectively signify the mixture viscosity and density, and their values are precisely defined as follows [19]:

$$\begin{aligned}\rho &= \gamma_\iota\rho_\iota + (1-\gamma_\iota)\rho_\vartheta \\ \mu &= \gamma_\iota\mu_\iota + (1-\gamma_\iota)\mu_\vartheta\end{aligned} \quad (7)$$

2.1 Volume of fluid (VOF) method

The Volume of Fluid (VOF) method reconstructs the interface between the vapor and liquid phases. The variable represents the fraction of fluid 1's volume and is subsequently determined [20]:

$$\gamma = \begin{Bmatrix} 1 & \text{fluid 1(Liquid)} \\ 0 & \text{fluid 2(Vapor)} \\ 0 < \gamma < 1 & \text{at the interface} \end{Bmatrix} \quad (8)$$

A compressive velocity (v_c) is incorporated into the prescribed VOF equation, as detailed in:

$$\frac{\partial\gamma}{\partial t} + \nabla.(\gamma\vec{u}) + \nabla.[\vec{u}_c\gamma(1-\gamma)] = \dot{\bar{m}} \quad (9)$$

The variable $\dot{\bar{m}}$ (kg/s) represents the normalized mass flow rate, determined according to the specific mass transfer model selected, following the approach of Kunz and Sauer. The term u_c denotes the compressive velocity component introduced in Rusche's study [21].

The VOF method offers several benefits for simulating cavitation phenomena. By combining a first-order limited downwind scheme with higher-order accurate schemes, it maintains a sharp fluid interface while minimizing numerical diffusion.

Moreover, the VOF method accurately predicts impact pressure caused by bubble collapse near a wall, which is vital for understanding bubble shape evolution. Many VOF implementations incorporate models for surface tension effects, crucial for determining bubble shapes. Studies by Ye et al. [19] and Zhang et al. [22] illustrate the VOF method's ability to predict cavitation impact and energy release from bubble collapse, underscoring its effectiveness in capturing bubble dynamics accurately. For a more detailed understanding of the compressive velocity Volume of Fluid (VOF) method, please consult the referenced works [23 ,24].

2.2 Large eddy simulation (LES)

In this study, the Large Eddy Simulation (LES) approach is utilized to model cavitating flows over a Clark-Y hydrofoil, focusing on resolving large-scale, energy-containing flow structures while modeling the smaller, isotropic sub grid scales. The implicit LES method leverages the truncation error of the numerical discretization as an inherent sub grid scale (SGS) model, eliminating the need for implicit filtering [25] . This approach, often termed "implicit LES, integrates the SGS modeling with the discretization scheme, where the finite volume method acts as an implicit top-hat filter. The filtered flow variable is expressed as:

$$\bar{f}_p = \frac{1}{(\delta V)p}\int \Omega_p\, f, dV \quad (10)$$

Here, $\overline{f_p}$ represents the filtered quantity over the cell volume $(\delta V)_p$ in the domain Ω_p.

2.3 Pressure-velocity coupling

ANSYS FLUENT employs the solution procedure based on the pressure implicit with splitting of operators (PISO) algorithm for coupling between pressure and velocity fields.

The PISO algorithm could be briefly described as follows Ref [24-26]:

1. Momentum prediction: First, the momentum equations are solved using a guessed pressure field, typically the pressure field from the previous time step. The solution of the momentum equations yields a new velocity field that does not satisfy the continuity condition. Additionally, the vapor volume fraction transport equation is solved in this step.

2. Pressure solution: The predicted velocities are utilized to solve the pressure equation, resulting in a new pressure field. The mass transfer terms are integrated into the pressure Poisson equation as a split source term.

3. Explicit velocity correction: The updated pressure field is utilized to explicitly adjust the velocity. The revised velocity aligns with the new pressure field. The velocity within a cell is influenced not only by the pressure gradient but also by contributions from adjacent cells. This iterative process persists until a predetermined tolerance is achieved.

3. Numerical approach

3.1 Discretization and geometry of the hydrofoil

In this section, modeling and structural meshing of the flow field is described. As the body of the shark is similar in shape to the wing structure of a hydrofoil, both are streamlined. Inspired by the shark gill slit breathing principle and jet structure, the gill slit structure can be applied to the hydrofoil Fig 1. As it is shown four various cases are considered i.e. Hydrofoil without jet injection (case1), Hydrofoil with 0.15c jet injection (case 2), Hydrofoil with 0.6c jet injection (case 3) and Hydrofoil with 0.6c and 0.15c jet injection (case 4). The features of its gill slit body surface are engineered and extracted, and the simplified jet structure is arranged on the surface of the hydrofoil to study the cavitation suppression of the hydrofoil surface by different bionic jet chord positions (according to Table1).

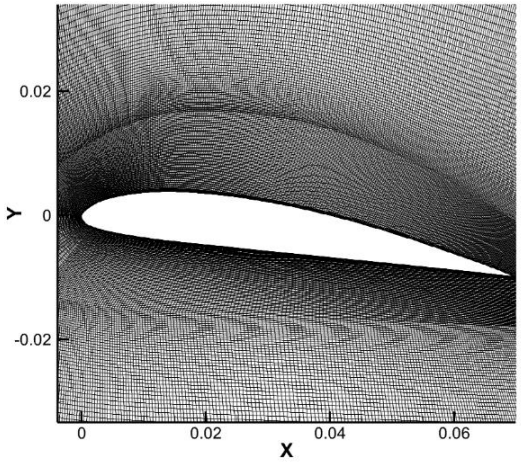

(a) case1

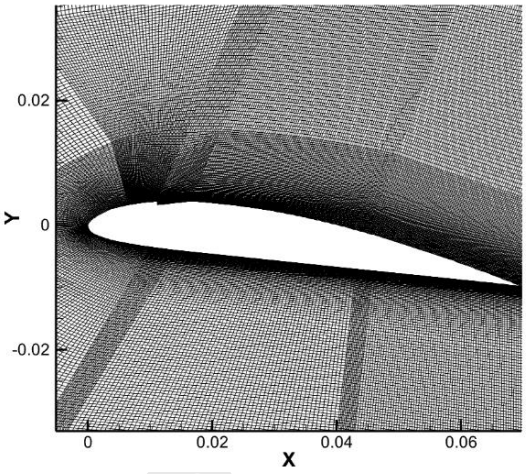

(b) case2

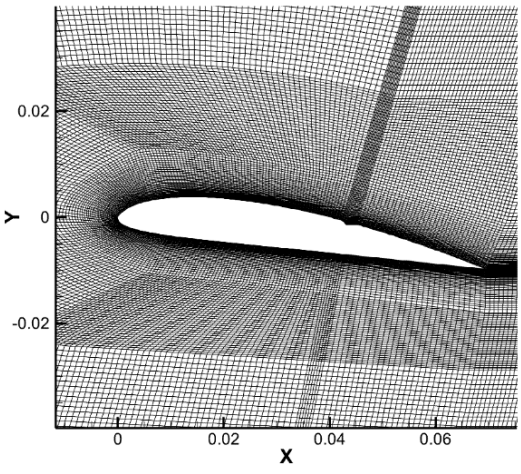

(c) case3

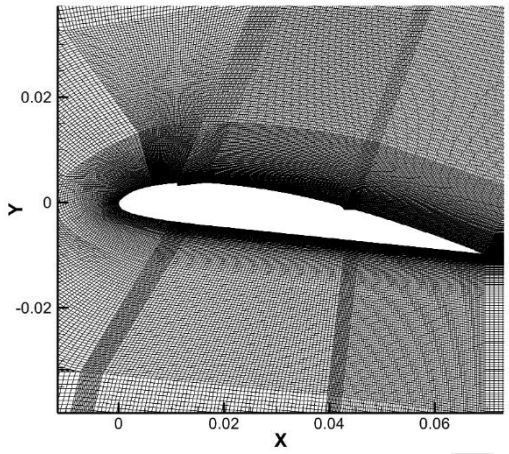

(d) case4

Fig 1. schematic of CLARK Y hydrofoil with corresponding grid.

Table 1. Schematic diagram of structural parameters of jet on the hydrofoil. (a) injection at 0.15c. (b) injection at 0.6c.

	X(mm)	Y(mm)
Injection at 0.15 chord	11.13	3.78
	11.13	3.21
	16.52	3.81

(a)

	X(mm)	Y(mm)
Injection at 0.6 chord	42.33	-0.59
	43.1	-7.08
	45.14	-1.37

(b)

3.2 Simulation set-up

The computational grids for the cases are illustrated in Fig. 1. Cases 1–4 consist of approximately 2.2×10^5 to 3.4×10^5 cells within the entire computational domain. The Clark-Y hydrofoil surface is discretized with about 200–250 cells on the upper side and 150–200 cells on the lower side. A structured mesh was generated using GAMBIT with a C-type topology, and a boundary layer grid growth rate of 1.15 was applied to ensure adequate near-wall resolution for laminar flow development at the leading edge. The jet velocity was initially set to $0.5U\infty$, aligned with the mainstream flow direction.

The computational domain and boundary conditions were established based on the experimental configuration described in Ref. [27]. The hydrofoil was positioned at the center of the water tunnel with an angle of attack of 8°, as shown in Fig. 2. The free-stream velocity was set to 10 m/s, corresponding to a Reynolds number of 7×10^5 for a chord length of 70 mm. A time step was chosen to maintain the Courant number below 0.45 throughout the domain [24]. The simulations were performed using the ANSYS Fluent solver in transient mode, with PISO pressure–velocity coupling to accurately capture the unsteady cavitating flow behavior. The transient simulations were iterated until the residuals of all governing equations dropped below 10^{-7}, ensuring numerical convergence and stability of the computed flow field.

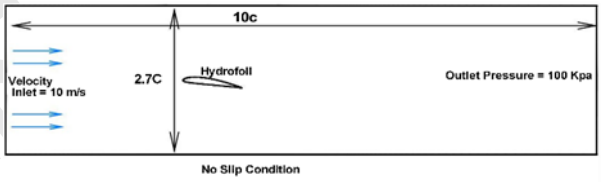

Fig. 2. Computational domain and boundary conditions.

4. Validation

To ensure the accuracy and reliability of the numerical simulations conducted in this study, the results have been meticulously validated against experimental data from Ref [27] and established numerical data from the literature, with particular reference to the work of Roohi et al. [24] The validation process focuses on key cavitation characteristics, including the inception point of cavitation, cavity morphology, lift and drag coefficients, and pressure distributions, for the Clark-Y hydrofoil under comparable flow conditions (cavitation number $\sigma = 0.8$, Reynolds number $Re = 7 \times 10^5$).

The present simulations employ the implicit Volume of Fluid (VOF) method coupled with the Large Eddy Simulation (LES) turbulence model, implemented within ANSYS Fluent. To validate the cavitation dynamics, the temporal evolution of cloud cavitation over the Clark-Y hydrofoil in the absence of jet injection (case 1) was compared with the experimental findings reported by Roohi et al. [24]. Their study documented the cavitation cycle for a cavitation number of σ=0.8 using the Schnerr-Sauer cavitation model.

The convergence of the unsteady simulations was carefully monitored to ensure a stable solution.

Fig. 3-a shows a typical history of the solver residuals for the simulation. For this transient LES/Note-VOF analysis, convergence is indicated by the residuals reaching a stable oscillatory pattern. This behavior represents a robust and fully converged solution for this complex multiphase simulation, confirming the stability of the numerical results presented. Ultimately, as it is shown in Fig.3-b the pressure coefficient distribution over the hydrofoil surface (case1) served as a suitable parameter for validating the numerical study in this paper, demonstrating good agreement with the results reported by Roohi et al[24].

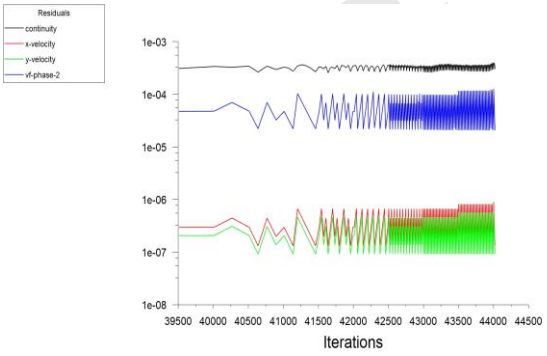

(a)

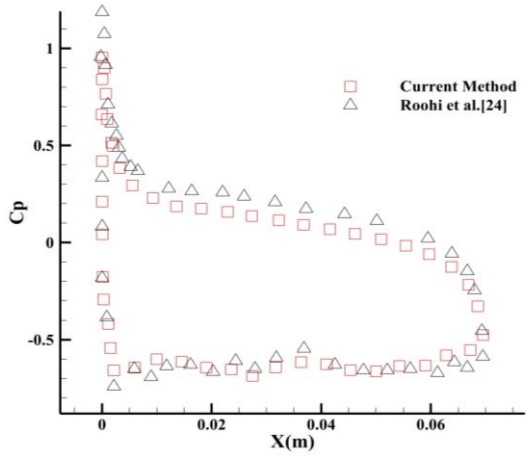

(b)

Fig. 3. (a): The convergence of the simulation (b): The comparison of our numerical solution for Cp with the numerical solution reported by Roohi et al.[24] is presented.

Moreover, Table.2 shows a comparison of the lift and drag coefficients with the experimental data from Reference 1 and the numerical results of Roohi et al.'s study revealed good agreement.

Table 2. The comparison of our numerical solution for Cl and Cd with the experimental study and Roohi et al. [24] numerical study is presented.

	C_L	C_d
Current study	0.75	0.110
Roohi et al.[15]	0.70	0.140
Experiment (No injection)	0.76	0.120
Deviation with experiment %	1.3	8.3

To provide a clearer comparison of the validation methodologies, the key numerical specifications of the current work and the reference study by Roohi et al. [24] are summarized in Table 3. As discussed in Section 4, these differences in the numerical setup, such as the solver platform and convergence stringency, contribute to the observed variations in the validation results presented in Table 2.

Table 3. Comparison of key numerical methodology specifications for validation.

Specification	**Current Study**	**Roohi et al. [24]**
CFD Platform	ANSYS Fluent	OpenFOAM
Grid Resolution (Base)	About 300000 cells	126840 cells
Near-Wall Meshing	Optimized boundary-layer	Boundary-layer
Convergence Criterion	Stringent Residuals < 10^{-7}	Not specified

5. Results and discussion

5.1 5.1 Analysis and comparison of pressure coefficient

Unsteady hydrofoil cavitation flow causes obvious fluctuations in the pressure coefficient at the suction surface. Fig 4 displays the pressure coefficient for all cases in the current study. Considering case 1 (without injection), a significant pressure drop near the leading edge (X<0.02 m) indicates severe cavitation. Injection at 0.15c mitigates the pressure drop effectively suppressing cavitation at the leading edge by enhancing local pressure. Conversely, injection at 0.6c primarily reduces cavitation near the trailing edge. The combined injection yields the most uniform pressure

distribution, minimizing cavitation across the hydrofoil surface.

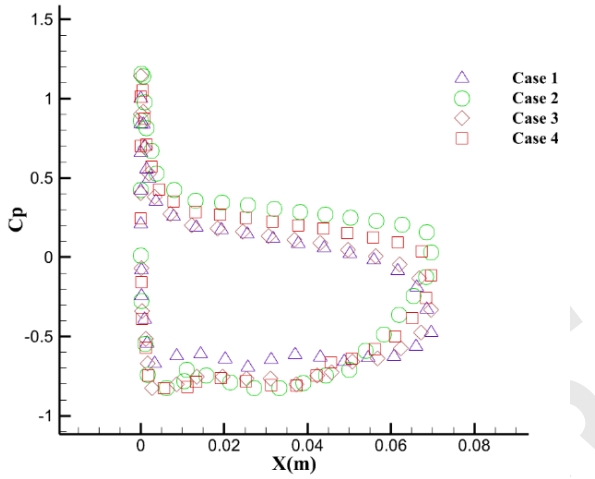

Fig. 4. pressure coefficient (Cp) distribution on a Clark-Y hydrofoil under various jet injection conditions

The Table.4. illustrates the variations of lift coefficient (C_L) and drag coefficient (C_d) for four jet injection cases. Furthermore, the volume fraction pf cavitation zone is illustrated in Fig.5 for different jet positions and time steps. For the case 2 with jet injection at 0.15c, lift coefficient has been decreased; while the drag has been increased. The reason can be stated by considering Fig.5 which shows volume fraction for all cases. Although using jet injection can vanish cavity at leading edge, it can make an impact on the cavity intensity at trailing edge.

Using jet engine at 0.6c (case 3), increases lift coefficient and drag coefficient simultaneously. (Table 4 and Fig5-e and Fig5-f). Interestingly, by using jet engine at 0.15c and 0.6c, the ratio C_L /C_d increases. The incremental percentage in this ratio is about 12 percent. As it is shown, in case 4, the big cavity has been changed into some small cavities which lead to increase of lift coefficient.

Table 4. Variation of lift and drag coefficient for all cases

	C_L	C_d	C_L /C_d
Case 1	0.75	0.110	6.81
Case 2	0.73	0.14٠	5.21
Case 3	0.82	0.12٠	6.83
Case 4	0.84	0.11٠	7.63

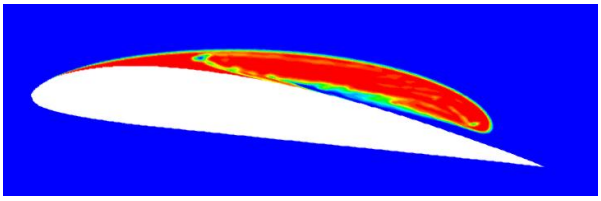

(a) Case 1 at time 17ms

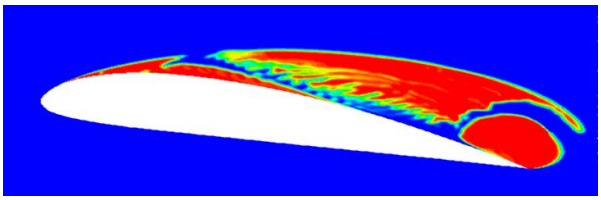

(b) Case 1 at time 21 ms

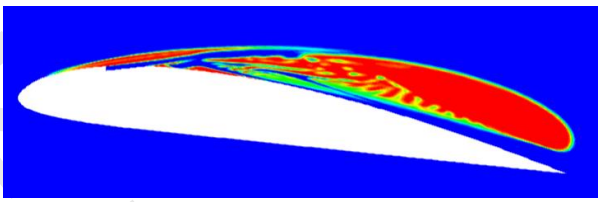

(c) Case 2 at time 17ms

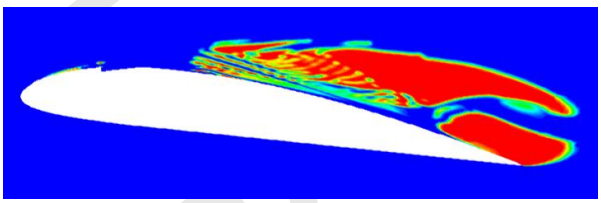

(d) Case 2 at time 21 ms

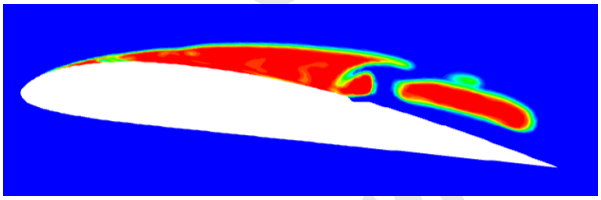

(e) Case 3 at time 17 ms

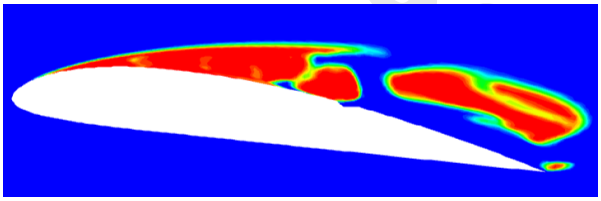

(f) Case 3 at time 21 ms

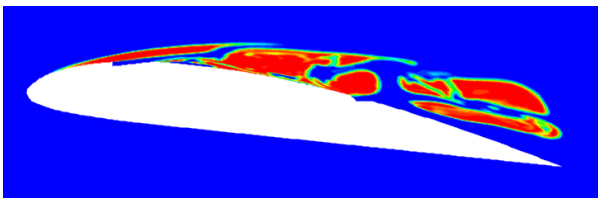

(g) Case 4 at time 17 ms

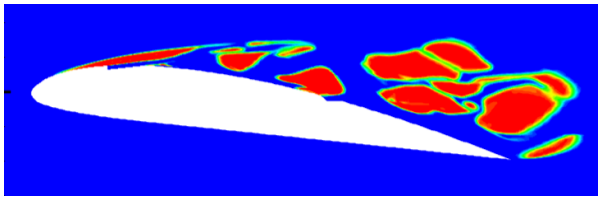

(h) Case 1 at time 21 ms

Fig 5. Volume fraction of all cases.

6. Conclusion

In this study, the cavitation phenomenon over a Clark-Y hydrofoil was numerically investigated to evaluate the effectiveness of jet injection in suppressing unsteady cavitation. By varying the jet positions at 0.15c, 0.6c, and a combined configuration (0.15c and 0.6c), the cavitation dynamics was analyzed using the implicit Volume of Fluid (VOF) method coupled with the Large Eddy Simulation (LES) turbulence model. The results demonstrate that jet injection significantly reduces the cavitation zone, with the injection at 0.15c being the most effective in minimizing the time averaged volume fraction and suppressing cloud cavitation near the leading edge. The combined jet configuration (0.15c and 0.6c) further enhances cavitation suppression, offering improved lift coefficient stability. Analysis of pressure and flow characteristics reveals that injections at 0.15c and 0.6c produce smaller, fragmented cavities compared to the case with no-injection case. These findings highlight the potential of bio-inspired jet injection, modeled after fish gill slits, to optimize hydrofoil performance by mitigating cavitation effects, providing valuable insights for the design of fluid machinery with enhanced durability and efficiency.

CONFLICTS OF INTEREST

The authors declare that they have no conflict of interest.

REFERENCES

[1] J. Sauer, “Instationär kavitierende strömungen - Ein neues modell, basierend auf front capturing (VoF) und blasendynamik,” Ph.D. dissertation, University of Karlsruhe, Karlsruhe, Germany, 2000, (in Germany).

[2] W. Yuan, J. Sauer, and G. H. Schnerr, “Modeling and computation of unsteady cavitation flows in injection nozzles,” *Mecanique & Industries*, vol. 2, no. 5, pp. 383–394, 2001.

[3] G. Wang and M. Ostoja-Starzewski, “Large eddy simulation of a sheet/cloud cavitation on a NACA0015 hydrofoil,” *Applied Mathematical Modelling*, vol. 31, no. 3, pp. 417–447, 2007, https://doi.org/10.1016/j.apm.2005.11.019

[4] T. Huuva, “Large eddy simulation of cavitating and non-cavitating flow,” Ph.D. dissertation, Chalmers University of Technology, Göteborg, Sweden, 2008.

[5] N. X. Lu, R. E. Bensow, and G. Bark, “LES of unsteady cavitation on the delft twisted foil,” *Journal of Hydrodynamics*, vol. 22, no. 1, pp. 742-749, 2010, https://doi.org/10.1016/S1001-6058(10)60031-5.

[6] P. Kumar, N. Sharma, S. K. Pattanayek, and A. Garg, “Computational comparison of passive control for cavitation suppression on cambered hydrofoils in sheet, cloud, and supercavitation regimes,” *Physics of Fluids*, vol. 36, no. 10, 2024, Art. no. 104113, https://doi.org/10.1063/5.0226200.

[7] Z. Wang, H. Cheng, B. Ji, and X. Peng, “Numerical investigation of inner structure and its formation mechanism of cloud cavitating flow,” *International Journal of Multiphase*, vol. 165, 2023, Art. no. 104484, https://doi.org/10.1016/j.ijmultiphaseflow.2023.104484.

[8] C. Mou, B. Che, Y. Wang, J. Zhang, L. Cao, and D. Wu, “Large eddy simulation of micro vortex generator-controlled cavitation across multiple stages,” *Physics of Fluids*, vol. 36, no. 10, 2024, Art. no. 10, https://doi.org/10.1063/5.0232189.

[9] J. Wang *et al.*, “Flow field characterization of cavitation water jets applied to concave, plane, and convex surfaces,” *Physics of Fluids*, vol. 37, no. 4, 2025, Art. no. 043309, https://doi.org/10.1063/5.0265218.

[10] Y. Long, X. Long, and B. Ji, “LES investigation of cavitating flows around a sphere with special emphasis on the cavitation–vortex interactions,” *Acta Mechanica Sinica*, vol. 36, no. 6, pp. 1238–1257, 2020, https://doi.org/10.1007/s10409-020-00993-w.

[11] A. K. Singhal, M. M. Athavale, H. Li, and Y. Jiang, “Mathematical basis and validation of the full cavitation model,” *Journal of Fluids Engineering,* vol. 124, no. 3, pp. 617–624, 2002, https://doi.org/10.1115/1.1486223

[12] C. Merkle, J. Feng, and P. Buelow, “Computational modeling of the dynamics of sheet cavitation,” in *3rd International Symposium on Cavitation*, Grenoble, France, 1998, pp. 307-313.

[13] R. F. Kunz *et al.*, “A preconditioned Navier-Stokes method for two-phase flows with application to cavitation prediction,” *Computers & Fluids*, vol. 29, no. 8, pp. 849–875, 2000, https://doi.org/10.1016/S0045-7930(99)00039-0.

[14]J. Li, H. Yan, and F. Wang, "Suppression of hydrofoil unsteady cavitation by periodic jets based on fish gill respiration," *Ocean Engineering*, vol. 293, 2024, Art. no. 116584, https://doi.org/10.1016/j.oceaneng.2023.116584.

[15] V. Viti, R. Neel, and J. A. Schetz, "Detailed flow physics of the supersonic jet interaction flow field," *Physics of* Fluids, vol. 21, no. 4, 2009, Art. no. 046101, https://doi.org/10.1063/1.3112736.

[16] M. Raeisi, M. Mohammadi-Amin, and R. Zakeri, "Numerical investigation of interaction of counter flow jet and hypersonic capsule flow via modified DsmcFoam," *ASME Journal of Heat and Mass Transfer*, vol. 141, no. 10, 2019, Art. no. 101703, https://doi.org/10.1115/1.4044150.

[17] K. Mahesh, "The Interaction of Jets with Crossflow," *Annual Review of Fluid Mechanics*, vol. 45, pp. 379-407, 2012, https://doi.org/10.1146/annurev-fluid-120710-101115.

[18]A. Kolahan, E. Roohi, and M. R. Pendar, "Wavelet analysis and frequency spectrum of cloud cavitation around a sphere," *Ocean Engineering*, vol. 182, pp. 235–247, 2019, https://doi.org/10.1016/j.oceaneng.2019.04.070.

[19]S. M. Mousavi and B. J. Lee, "Investigation of bubble structure in a microchannel under microgravity conditions: Effects of discontinuous wettability with dynamic contact angle," *Acta Astronautica*, vol. 201, pp. 394–400, 2022, https://doi.org/10.1016/j.actaastro.2022.09.048.

[20]S. M. Mousavi, F. Sotoudeh, B. J. Lee, M. R. Paydari, and N. Karimi, "Effect of hybrid wall contact angles on slug flow behavior in a T-junction microchannel: A numerical study," *Colloids and Surfaces A: Physicochemical and Engineering Aspects*, vol. 650, 2022, Art. no. 129677, https://doi.org/10.1016/j.colsurfa.2022.129677.

[21]H. Runrik, "Computational fluid dynamics of dispersed two-phase flow at high phase fractions," Ph.D. dissertation, University of London, London, United Kingdom, 2002.

[22] J. Zhang, L. Zhang, and J. Deng, "Numerical study of the collapse of multiple bubbles and the energy conversion during bubble collapse," *Water*, vol. 11, no. 2, 2019, Art. no. 247, https://doi.org/10.3390/w11020247.

[23]J. Klostermann, K. Schaake, and R. Schwarze, "Numerical simulation of a single rising bubble by VOF with surface compression," *International Journal for Numerical Methods in Fluids*, vol. 71, no. 8, pp. 960–982, 2013, https://doi.org/10.1002/fld.3692.

[24] E. Roohi, A. P. Zahiri, and M. Passandideh- Fard, "Numerical simulation of cavitation around a two-dimensional hydrofoil using VOF method and LES turbulence model," *Applied Mathematical Modelling*, vol. 37, no. 9, pp. 6469–6488, 2013, https://doi.org/10.1016/j.apm.2012.09.002.

[25]R. E. Bensow and G. Bark, "Simulating cavitating flows with LES in OpenFOAM," in *V European Conference on Computational Fluid Dynamics*, Lisbon, Portugal, 2010, pp. 14–17.

[26] R. I. Issa, "Solution of the implicitly discretised fluid flow equations by operator-splitting," *Journal of Computational Physics*, vol. 62, no. 1, pp. 40–65, 1986, https://doi.org/10.1016/0021-9991(86)90099-9.

[27]G. Wang, I. Senocak, W. Shyy, T. Ikohagi, and S. Cao, "Dynamics of attached turbulent cavitating flows," *Progress in Aerospace Sciences*, vol. 37, no. 6, pp. 551–581, 2001, https://doi.org/10.1016/S0376-0421(01)00014-8.

[28]B. Huang and G. Y. Wang, "Partially averaged Navier-Stokes method for time-dependent turbulent cavitating flows," *Journal of Hydrodynamics*, vol. 23, no. 1, pp. 26–33, 2011, https://doi.org/10.1016/S1001-6058(10)60084-4.